TURUN YLIOPISTON JULKAISUJA
ANNALES UNIVERSITATIS TURKUENSIS

SARJA - SER. A I OSA - TOM. 467

ASTRONOMICA - CHEMICA - PHYSICA - MATHEMATICA

STUDIES OF SOLAR ACTIVITY WITH EMPHASIS ON QUASI-PERIODIC OSCILLATIONS

by

Juha Kallunki

TURUN YLIOPISTO
UNIVERSITY OF TURKU
Turku 2013

From

Department of Physics and Astronomy
University of Turku
FI-20014 Turku
Finland

Supervised by

Alexandr Riehokainen
Senior researcher
Department of Physics and Astronomy
University of Turku
Finland

Reviewed by

Kiyoto Shibasaki
Professor
Nobeyama Radio Observatory
National Astronomical Observatory of Japan
Japan

Alexander Stepanov
Professor
Russian Academy of Sciences
Pulkovo Observatory
Russia

Opponent

Arnold O. Benz
Professor (Emeritus)
Institute for Astronomy
ETH Zurich
Switzerland

ISBN 978-951-29-5466-7 (PRINT)
ISBN 978-951-29-5467-4 (PDF)
ISSN 0082-7002
Painosalama Oy - Turku, Finland 2013

Acknowledgements

First of all, I would like to thank my supervisor Dr. Alexandr Riehokainen for valuable comments and advice, without him this project could not be possible. I am also grateful to my thesis director Prof. Esko Valtaoja, pre-examiners; Prof. Alexander Stepanov and Prof. Kiyoto Shibasaki. I have had a privilege to work with a solar (radio) physics with several researchers, I would like to thank all of them, especially all co-authors. Additionally, I would like to thank Metsähovi Radio Observatory crew for the various support over these years.

However, the biggest compliment goes to the loved ones:

> *"Vanhemmilleni, ja niille, jotka äänestivät Urho Kaleva Kekkosta vuoden 1956 presidentinvaaleissa."* (Vapaa lainaus (muunnellen) tohtori Lasse Lehtisen väitöskirjasta: "Aatosta jaloa ja alhaista mieltä. Urho Kekkosen ja SDP:n suhteet 1944-1981", 2002)

I have spent countless hours of my free time during this project, and now, it is a time for something totally else and a moment to follow instruction given by Olavi Paavolainen:

> *"Maassa ei ole lainkaan kastetta. Makaan pitkään ruohikossa ja seurustelen erään metsätähden kanssa."* (Synkkä yksinpuhelu, 1946)

Juha Kallunki,
Helsinki, 2013

Contents

Abstract

In this thesis mainly long quasi-periodic solar oscillations in various solar atmospheric structures are discussed, based on data obtained at several wavelengths, focussing, however, mainly on radio frequencies. Sunspot (Articles II and III) and quiet Sun area (QSA) (Article I) oscillations are investigated along with quasi-periodic pulsations (QPP) in a flaring event with wide-range radio spectra (Article IV). Various oscillation periods are detected; 3–15, 35–70 and 90 minutes (QSA), 10-60 and 80-130 minutes (in sunspots at various radio frequencies), 3-5, 10-23, 220-240, 340 and 470 minutes (in sunspots at photosphere) and 8-12 and 15-17 seconds (in a solar flare at radio frequencies). Some of the oscillation periods are detected for the first time, while some of them have been confirmed earlier by other research groups. Solar oscillations can provide more information on the nature of various solar structures.

This thesis presents the physical mechanisms of some solar structure oscillations. Two different theoretical approaches are chosen; magnetohydrodynamics (MHD) and the shallow sunspot model. These two theories can explain a wide range of solar oscillations from a few seconds up to some hours. Various wave modes in loop structures cause solar oscillations ($<$ 45 minutes) both in sunspots and quiet Sun areas. Periods lasting more than 45 minutes in the sunspots (and a fraction of the shorter periods) are related to sunspot oscillations as a whole. Sometimes similar oscillation periods are detected both in sunspot area variations and respectively in magnetic field strength changes. This result supports a concept that these oscillations are related to sunspot oscillations as a whole. In addition, a theory behind QPPs at radio frequencies in solar flares is presented.

The thesis also covers solar instrumentation and data sources. Additionally, the data processing methods are presented. As the majority of the investigations in this thesis focus on radio frequencies, also the most typical radio emission mechanisms are presented. The main structures of the Sun, which are related to solar oscillations, are also presented. Two

separate projects are included in this thesis. Solar cyclicity is studied using the extensively large solar radio map archieve from Metsähovi Radio Observatory (MRO) at 37 GHz, between 1978 and 2011 (Article V) covering two full solar cycles. Also, some new solar instrumentation (Article VI) was developed during this thesis.

List of papers

This thesis consists of a review of the subject and the following original research articles:

I **The statistical study of quasi-periodic oscillations of the radio emission in solar quiet regions**,
J. Kallunki, and A. Riehokainen, Astronomische Nachrichten **333**, 20 (2012).

II **Long-period oscillations of millimeter emission above sunspots**,
V. Smirnova, A. Riehokainen, V. Ryzhov, A. Zhiltsov, and J. Kallunki, A&A **534**, A137 (2011).

III **Investigations of the quasi-periodic solar oscillations in sunspots based on SOHO/MDI magnetograms**,
J. Kallunki, and A. Riehokainen, Sol. Phys. **116**, 10.1007/s11207-012-0021-x (2012).

IV **Radio pulsating structures with coronal loop contraction**,
J. Kallunki, and S. Pohjolainen, Sol. Phys. **101**, 10.1007/s11207-012-0003-z (2012).

V **A study of long-term solar activity at 37 GHz**,
J. Kallunki, N. Lavonen, E. Järvelä, and M. Uunila, Baltic Astronomy **21**, 255 (2012).

VI **Callisto radio spectrometer for observing the Sun - Metsähovi Radio Observatory joins the worldwide observing network**,
J. Kallunki, C. Monstein, and M. Uunila, IIEEE Aerospace and Electronics Systems Magazine **August 2013**, p.5-9 (2013).

List of abbreviations

AR - active region
BMSTU - Bauman Moscow State Technical University (Russia)
CALLISTO - Compound Astronomical Low-cost Low-frequency Instrument for Spectroscopy and Transportable Observatory
CME - Coronal Mass Ejection
CSHKP - Solar flare model developed by Carmichael, Sturrock, Hirayama, Kopp and Pneuman
GPS - Global Position System
GWS - Global Wavelet Spectrum
DPS - Drifting Pulsating Source
GBSRBS - Green Bank Solar Radio Burst Spectrometer
HMI - Helioseismic and Magnetic Imager
ETHZ - Eidgenössische Technische Hochschule Zürich (Switzerland)
EUV - extreme-ultraviolet
FFT- Fast Fourier Transform
MATLAB - The Language of Technical Computing
MDI - Michelson Doppler Imager
MHD - magnetohydrodynamic
MRO - Metsähovi Radio Observatory (Finland)
NOAA - The National Oceanic and Atmospheric Administration (USA)
NoRH - Nobeyama Radioheliograph (Japan)
NRH - Nancay Radioheliograph (France)
QPP - Quasi-Periodic Pulsation
QSA - Quiet Sun Area
QSJ - Quiet Sun Jets
QSL - Quiet Sun Level
RFI - Radio Frequency Interference
RT - radiotelescope
SOHO - The Solar and Heliospheric Observatory
SDO - Solar Dynamics Observatory

SST - Swedish Solar Telescope (Spain)
TV - television
UTC - Coordinated Universal Time
UV - ultraviolet

Chapter 1

The Sun

1.1 General information about the Sun

The Sun is the nearest star, the center of our Solar System. The mass of the Sun is 1.9891 x 10^{30} kg (333 000 x Earth), the majority of which is hydrogen (about 75 %) and helium (about 25 %), with the remainder being a combination of oxygen, carbon, neon, iron etc. The density at the photosphere is about 2 x 10^{-4} kg/m^3. The equatorial radius of the Sun is 6.955 x 10^5 km (109 x Earth). Constant nuclear fusion reactions create a huge amount of energy in the Sun. The radiation of the Sun can be observed in a wide spectral range. The radiation spectrum of the Sun is presented in Figure 1.1.

Sunspot magnetic cycle

Sunspots have an 11-year cycle, thus every 11th year (on average) we will see a maximum number of sunspots and various solar activity, and respectively a minimum every 11th year. This periodic behaviour is related to changes in the magnetic field of the Sun, more precisely to changes in the magnetic field polarity (the solar magnetic cycle is 22 years). The results of observations presented in this thesis have been made primarily during solar cycles 23 (1996-2008) and 24 (2008-), capturing periods of both minimum and maximum activity.

1.2 Structure of the Sun

The solar atmosphere consists of three different main layers: the photosphere, the chrosmosphere and the corona. Figure 1.2 illustrates the

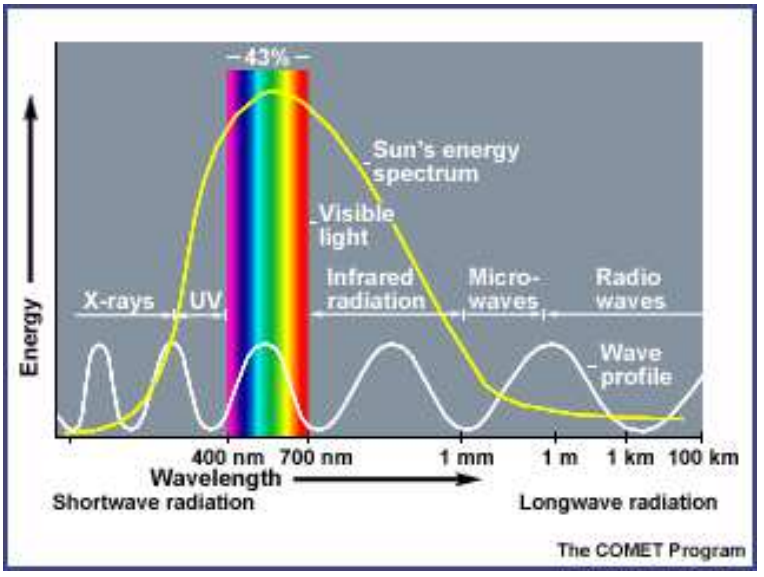

Figure 1.1: Radiation (energy) spectrum of the Sun [UCAR].

temperature variation in the different solar atmospheric layers. The photosphere is a thin layer, only about 500 km. Most of the Sun's visible light (shown in Figure 1.1) comes from the photosphere. The most typical structure in the photosphere is the solar granulation. This structure is caused by continuously moving plasma from the solar interior to the photosphere. The size of a solar granule can be as large as 1000 km. Additionally, larger structures, so-called super granulae, with diameters measuring up to $\sim$ 30,000 km, can also be found. Strong magnetic field (1-2 kG) structures can be found at the boundaries of supergranulae ([Lou 1995]; [Anzer and Galloway 1983]). At these boundaries footpoints of various flux tube features can be observed, which can be either open and closed loop structures. The flux tubes are highly magnetic structures. And, furthermore, flux tubes are one source of solar oscillations. Granulae are not static structures.

The most significant features in the photospheric level are sunspots. The sunspots are visible at optical wavelengths. They are cooler (3000-4000 K) than the surrounding area of the surface (about 6000 K). The visible size of the sunspot can be as large as 80000 km. It is an extremely

magnetic structure (the magnetic field strength can be over 4 kG), which consists of an umbra (with a vertical magnetic field) and a penumbra (with a horizontal magnetic field). Sunspots are regularly visible in pairs (with positive and negative polarities), which are usually connected by a systems of loops. The loops can also connect two separate sunspot groups together. Some solar events (etc., solar flares) are usually closely related to sunspots. The sunspots are not static structures. Their lifetimes vary from a few hours to several weeks. Also, various solar oscillation periods have been observed in sunspots. Several observations at various wavelengths (such as optical), and also in magnetograms, give us detailed information of the photosphere. Physical models for sunspots are discussed in Chapter 3.

The chromosphere is a thin layer (around 2000 km) between the photosphere and the transition region, where temperature varies between 4200 and 8000K. The most typical features in the chromosphere are spicules, however they can be observed as high as about 5000 km [Stix 2004]. The most common data obtained from the chrosmospheric level are CaII and Hα spectral lines.

The outer layer, the corona, is a hot structure, which extends a million kilometers into space. Various loop structures are visible in the corona (coronal loop structures). Different eruption events (solar flares and coronal mass ejections, CMEs) are also visible in the chromosphere and in the corona. Radio observations enable us to study the chromosphere, the transition region and the corona. Another feature in the corona is a coronal hole. The coronal holes are open magnetic field structures. They are areas of low temperature and density in comparison with the surrounding area.

1.3 Energy transport of the Sun

The solar interior has three main layers: the core, the radiative zone and the convective zone. In the core, nuclear reactions take place and most of the energy originates there. Energy from the core is transmitted towards the surface by radiation in the radiation zone; beyond that, energy is transmitted towards the surface via convection by plasma in the convective zone. In Figure 1.3, the Sun's structure and common physical phenomena are shown. The temperature in the center of the Sun is around 1.2 x 10^7 K, and on the surface it is around 6000 K, while the corona is a very hot structure. Several mechanisms cause coronal heating, mainly various reconnection processes

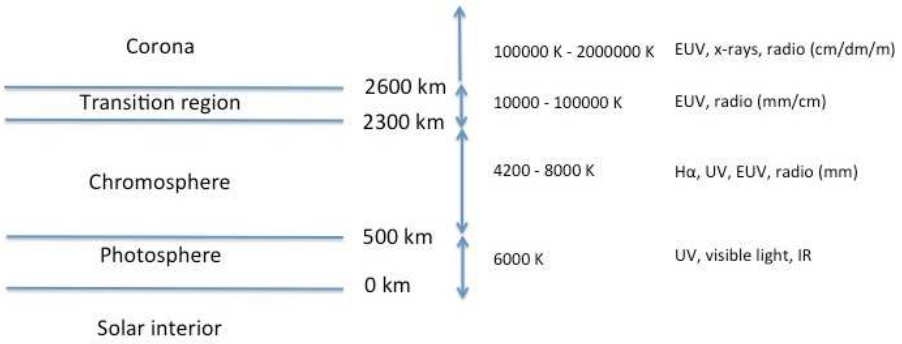

Figure 1.2: Temperature variation of different solar atmospheric layers.

and waves (such as acoustic and Alfven waves) [Aschwanden 2006].

1.4 Solar events - solar flares

Massive releases of energy (up to 6×10^{25} J) in the magnetic structures are called solar flares. These events eject a huge amount of electrons and ions into space. Usually, it is possible to detect these events across the electromagnetic spectrum. These flaring events also include pulsating phenomena, at radio and other wavelengths. A standard solar flare model (also known as the Shibata or the extended CSHKP model) is presented in Figure 1.4. (left) The model also shows features of solar flares in soft and hard X-rays. Typically, a solar flare consists of three phases: a precursor (soft X-rays), an impulsive phase (hard X-rays, radio) and a gradual phase (soft X-rays, Hα and post-flare loops). The magnetic reconnection takes place above closed loops, further generating outgoing plasmoids (jet outflows away from the Sun) and reconnection outflow jets. These outflow jets cause termination shocks when they collide with a loop arcade [McKenzie 2002].

Usually, solar flares are associated with ejected plasmoids, including secondary plasmoids. Drifting pulsating structures of the radio emission (DPS in Figure 1.4, right) are generated by electron beams, which are injected into the plasmoid during the reconnection process. The motion of the plasmoids determines the drifting pattern of the oscillation structures. With an increased drift frequency comes an increased reconnection rate.

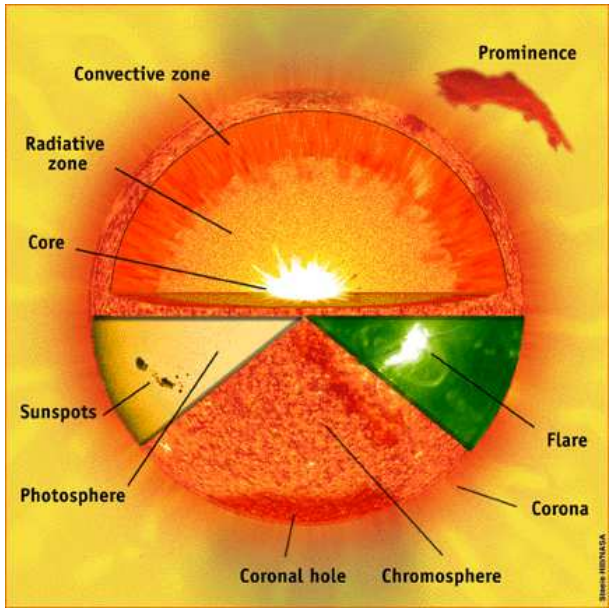

Figure 1.3: Structure of the Sun. The three main inner layers of the Sun are the core, the radiative zone and the convective zone. The atmospheric layers are the photosphere, the chromosphere and the corona [CNES].

The model by [Karlicky and Barta 2004] can explain the decimetric DPS.

Another interpretation for quasi-periodic pulsations (QPP) is proposed by [Nakariakov et al. 2006]. They assume that the cooler loop, situated near a flaring arcade, provides fast magnetoacoustic oscillations (a theory of which is presented in Chapter 2), which are capable of leaking a part of the oscillations to a magnetic null point in the arcade, modulating the current density and triggering magnetic reconnection. This periodically accelerates particles which follow the field lines and precipitate in the dense atmosphere, causing quasi-periodic emission at various wavelengths, including radio wavelengths.

1.5 Solar oscillations

During the recent decades with better observational capabilities, a major research topic in solar astronomy has been helioseismology and solar os-

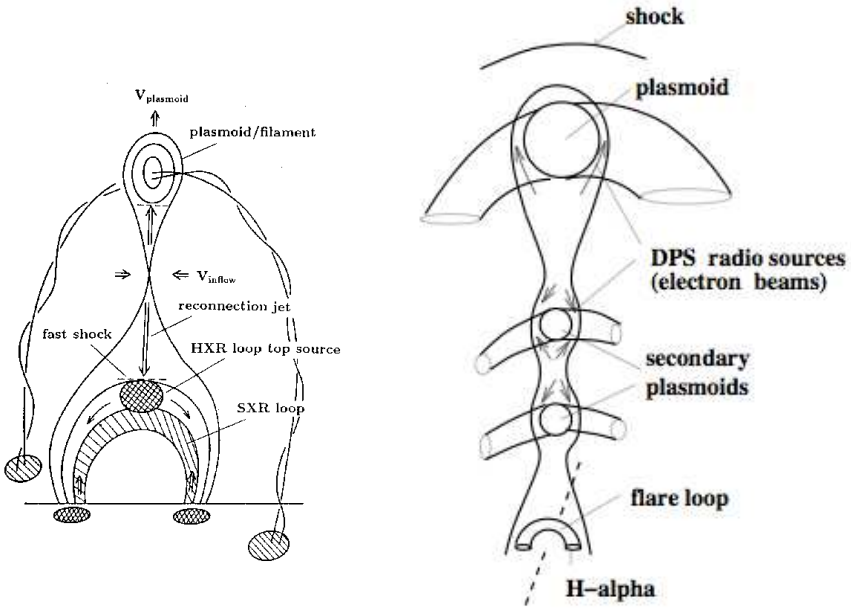

Figure 1.4: Left. A standard flare model by [Shibata and Magara 2011], Right. A model for QPP in solar flare by [Karlicky and Barta 2004].

cillations of different solar structures (local helioseismology). Perhaps the most well-known and studied object in this sense is the sunspot. Oscillatory events have been investigated at various wavelengths including UV, radio and optical. Various oscillation periods have been found and, in part, the results have even been contradictory.

1.5.1 Helioseismology

Helioseismology mainly studies the acoustic wave oscillations in the Sun, which are generated in the solar interior and further are moving towards the surface. These waves are divided into three categories based on the restoring force: the p-, g-, and f-modes (pressure, gravity and surface gravity). A well-known oscillation has a 5-minute period, discovered already in the early 1960s by [Leighton et al. 1962]. They assumed that this oscillation was related to the turbulent motion in the convective zone of the Sun. Helioseismology (oscillations) can, for example, provide new infor-

mation about the solar structures and dynamics such as the temperature distribution, the chemical composition and the internal rotation

1.5.2 Local helioseismology

As was mentioned, during the past couple of years a lot of different studies have been published on solar oscillations in different solar atmospheric structures (local helioseismology). Oscillation periods in different solar structures, detected in these studies, are listed in table 1.1. Long quasi-periodic oscillations, such as those reported in this thesis, can provide, for instance, new information or improvements on the prevailing interpretations about the sunspot magnetic field structure.

Table 1.1 shows several oscillation periods from a few minutes up to several hours even in the same solar structures as detected by various researches during the last few years. Thus, the detected oscillations illustrate various physical phenomena, and they might offer new approaches to, for example, the sunspots' physical processes. In this thesis, solar oscillations in quiet Sun areas and sunspots are studied mainly at radio wavelengths and at periods between 3 minutes and 5 hours.

Solar oscillations (quasi-periodic pulsations lasting about 5-20 seconds) in solar flares at radio wavelengths are also discussed.

Table 1.1: List of recently detected (published) solar oscillation periods in different solar structures at various wavelengths.

	Object	Wavelength	Periods
[Kallunki and Riehokainen 2012]	quiet Sun area	17 GHz	3–15, 35–70, 90 min
[Kallunki and Riehokainen 2012]	sunspot	magnetogram	3-5, 10-23, 220-240, 340, 470 min
[Smirnova et al. 2011]	sunspot	17 GHz, 37 GHz, 93 GHz	10-60, 80-130 min
[Abramov-Maximov et al. 2011]	sunspot/AR	17 GHz, Hα	160-200 s, 15-16, 30-32 min
[Dzhimbeeva 2011]	sunspot	17 GHz	3-5, 25-80, 90-110, 120-140, 160-210 min
[Efremov et al. 2011]	sunspot	magnetogram	40-45, 60-80, 135-170, 220-240, 460-500 min
[Martinez Gonzalez et al. 2011]	quiet Sun area	magnetogram	5-20 min
[Kontogiannis et al. 2010]	quiet Sun area	Hα, Ca II, TRACE (1550 Å, 1600 Å, 1700 Å), magnetogram	3, 5, 7 min
[Andic et al. 2010]	quiet Sun area	TiO (705.68 nm)	30-120 s, 4.3 min
[Kariyappa and Dame 2010]	quit Sun area	TRACE (1600 Å)	3.4, 4.6, 5.5 h
[Asai et al. 2012]	prominence/filament	Hα, EUV	12-16 min
[Chorley et al. 2010]	sunspot	17 GHz	16-88 min

Chapter 2

Magnetohydrodynamics

2.1 Magnetohydrodynamics (MHD)

Magnetohydrodynamics (MHD) defines the behaviour of plasma in a magnetic field. MHD theory enables us to understand the active phenomena of the Sun, such as sunspots and solar flares. Based on the MHD theory, it is possible to derive equations for various wave types (speeds) in a plasma; Alfven, sound, and slow and fast MHD waves. Based on them we can define various oscillation periods in different solar magnetic field structures. All waves result from restoring forces; magnetic tension, gas and/or magnetic pressure. However, the MHD equations presented here do not take into account gravity. The equations presented here follow [Aschwanden 2006].

2.1.1 Maxwell and hydrodynamic equations

The Maxwell equations (differential form, equations 2.1 - 2.4) describe the relation between the electric field (**E**), the magnetic field (**B**), the charge density (ρ) and the current (**J**).

$$\nabla \cdot \mathbf{E} = \frac{\rho}{\epsilon_0} \text{ (Gauss's law)} \tag{2.1}$$

$$\nabla \cdot \mathbf{B} = 0 \text{ (Gauss's law for magnetism)} \tag{2.2}$$

$$\nabla \times \mathbf{E} = -\frac{\partial \mathbf{B}}{\partial t} \text{ (Faraday's law)} \tag{2.3}$$

$$\nabla \times \mathbf{B} = \mu_0 \mathbf{J} + \mu_0 \epsilon_0 \frac{\partial \mathbf{E}}{\partial t} \text{ (Ampere's law)} \tag{2.4}$$

where $\nabla = \mathbf{x}\frac{\partial}{\partial x} + \mathbf{y}\frac{\partial}{\partial y} + \mathbf{z}\frac{\partial}{\partial z}$ (in Cartesian coordinates) and μ_0 is permeability in a vacuum. Additionally, we have taken into consideration Ohm's law.

$$\mathbf{J} = \sigma(\mathbf{E} + \mathbf{v} \times \mathbf{B}) \text{ (Ohm's law)} \tag{2.5}$$

where σ is the conductivity. Often, we can assume that σ is very large, thus we can use the ideal Ohm's law

$$\mathbf{E} + \mathbf{v} \times \mathbf{B} = 0 \text{ (ideal Ohm's law)} \tag{2.6}$$

where $\mathbf{v}$ is the velocity of the mass center (bulk plasma velocity). Also, we take into consideration the hydrodynamic equations

$$\frac{\partial \rho}{\partial t} + \nabla \cdot (\rho_m \mathbf{v}) = 0 \text{ (continuity)} \tag{2.7}$$

$$\rho_m \frac{\partial \mathbf{v}}{\partial t} + \rho_m (\mathbf{v} \cdot \nabla)\mathbf{v}) = -\nabla p + \mathbf{J} \times \mathbf{B} \text{ (momentum)} \tag{2.8}$$

$$\nabla p = v_s^2 \nabla \rho \text{ (energy)} \tag{2.9}$$

where v_s is the local sound speed, p is the pressure and ρ_m is the mass density. Now we can combine equations 2.4 (Ampere's law) and 2.9 (energy)

with equation 2.8.

$$\rho_m \frac{\partial \mathbf{v}}{\partial t} + \rho_m(\mathbf{v} \cdot \nabla)\mathbf{v}) = -v_s^2 \nabla \rho_m + (\nabla \times \mathbf{B}) \times \mathbf{B}/\mu \tag{2.10}$$

We can also combine equations 2.3 (Faraday's law) and 2.6 (ideal Ohm's law).

$$\nabla \times (\mathbf{v} \times \mathbf{B}) = \frac{\partial \mathbf{B}}{\partial t} \tag{2.11}$$

The Alfven speed is defined as

$$v_A = \sqrt{\frac{B^2}{\mu_0 \rho_m}} \tag{2.12}$$

The Alfven wave propagates along the magnetic field and the only prevailing force is the magnetic field tension.

2.1.2 Linearized MHD equations

Each parameter consist of a part, which is constant both in time and space, and also of a part which is varying. Thus, the variables should be linearised and re-written. Taking into account the second order (or higher) terms, the equations would become very challenging to solve.

$$\begin{aligned} \mathbf{B}(\mathbf{r},t) &= \mathbf{B_o} + \mathbf{B_1}(\mathbf{r},t) \\ \rho_\mathbf{m}(\mathbf{r},t) &= \rho_\mathbf{m0} + \rho_\mathbf{m1}(\mathbf{r},t) \\ \mathbf{v}(\mathbf{r},t) &= \mathbf{v_o} + \mathbf{v_1}(\mathbf{r},t) \end{aligned} \tag{2.13}$$

Now, we should re-write equations 2.7 (continuity), 2.10 and 2.11 using lineriazed varibles, assuming that the second order terms are small. Then equations can then be written

$$\begin{aligned} \frac{\partial \rho_{m1}}{\partial t} + \nabla \cdot (\rho_{m0} \mathbf{v_1}) &= 0 \\ \rho_{m0} \frac{\partial \mathbf{v_1}}{\partial t} + v_s^2 \nabla \rho_{m1} + \mathbf{B_0} \times (\nabla \times \mathbf{B_1})/\mu &= 0 \\ \frac{\partial \mathbf{B_1}}{\partial t} - \nabla \times (\mathbf{v_1} \times \mathbf{B_0}) &= 0 \end{aligned} \tag{2.14}$$

In order to find the equation for $\boldsymbol{v_1}$, we can first take the time derivate of the middle equation:

$$\rho_{m0} \frac{\partial^2 \mathbf{v_1}}{\partial^2 t} + v_s^2 \nabla (\frac{\partial \rho_{m1}}{\partial t}) + \frac{\mathbf{B_0}}{\mu} \times (\nabla \times \frac{\partial \mathbf{B_1}}{\partial t}) = 0 \tag{2.15}$$

Now we can combine equations 2.14 (upper and lower) and 2.12 with equation 2.15. We get

$$\frac{\partial^2 \mathbf{v_1}}{\partial^2 t} + v_s^2 \nabla (\nabla \cdot \mathbf{v_1}) + \mathbf{v_A} \times (\nabla \times (\nabla \times (\mathbf{v_1} \times \mathbf{v_A}))) = 0 \tag{2.16}$$

where $\mathbf{v_A}$ is the Alfven velocity (equation 2.12) as a vector. Finally, we have to find plane wave solutions by writing

$$\mathbf{v}(\mathbf{r}, t) = \mathbf{v_1} e^{[i(\mathbf{k} \times \mathbf{r} - \omega t)]} \tag{2.17}$$

Additionally, we have to replace the derivatives, $\nabla \rightarrow i\mathbf{k}$ and $\frac{\partial}{\partial t} \rightarrow -i\omega$, converting equation for $\mathbf{v_1}$ into an algebraic dispersion relation. Then we can write the final dispersion relation

$$\begin{aligned} -\omega^2 \mathbf{v_1} + (v_s^2 + v_A^2)(\mathbf{k} \times \mathbf{v_1})\mathbf{k} \\ +(\mathbf{k} \times \mathbf{v_A})[(\mathbf{k} \times \mathbf{v_A})\mathbf{v_1} - (\mathbf{v_A} \times \mathbf{v_1})\mathbf{k} - (\mathbf{k} \times \mathbf{v_1})\mathbf{v_A}] = 0 \end{aligned} \tag{2.18}$$

This equation 2.18 gives solutions for all ideal MHD wave modes.

2.1.3 MHD modes

Finally, we can write equations for the five main wave types, which enable us to derive the main oscillation periods in the magnetic field structures.

Magnetoacoustic (magnetosonic) wave

Case: $\mathbf{k} \perp \mathbf{B_0} \rightarrow \mathbf{k} \cdot \mathbf{v_A} = 0$

$$\frac{\omega}{k} = \sqrt{v_s^2 + v_A^2} \tag{2.19}$$

Sound wave

Case: $\mathbf{k} \parallel \mathbf{B_0} \rightarrow \mathbf{k} \cdot \mathbf{v_A} = kv_a, \mathbf{v_1} \parallel \mathbf{B_0} \parallel \mathbf{k} \rightarrow \mathbf{v_1} \parallel \mathbf{v_A} \rightarrow \mathbf{v_1} \cdot \mathbf{v_A} = v_1 v_A$

$$\frac{\omega}{k} = v_s \tag{2.20}$$

Alfven wave

Case: $\mathbf{k} \parallel \mathbf{B_0} \rightarrow \mathbf{k} \cdot \mathbf{v_A} = kv_a, \mathbf{v_1} \perp \mathbf{B_0} \parallel \mathbf{k} \rightarrow \mathbf{v_1} \cdot \mathbf{v_A} = 0$

$$\frac{\omega}{k} = v_A \tag{2.21}$$

Slow and fast MHD waves

The equation for the fast (+ sign) and the slow (- sign) wave can be solved by assuming that perturbations are proportional to $e^{i(\omega t + k_x x + k_z z)}$) [Whang 1997].

$$(\frac{\omega}{k})^2 = \frac{1}{2}(v_s^2 + v_A^2) \pm [(v_s^2 + v_A^2)^2 - 4v_s^2 v_A^2 cos^2\theta]^{\frac{1}{2}} \tag{2.22}$$

where θ is the angle between $\mathbf{k}$ and $\mathbf{B}$.

2.1.4 MHD oscillations

The different oscillation periods (modes) in the magnetic field loops (such as the coronal loop) can be calculated based on the wave types presented above. A typical coronal loop length (L) is 100 Mm [Roberts 2000] and the loop length can be as large as 300 Mm [Nakariakov and Stepanov 2007]. Therefore, the oscillation period (τ) can be calculated as

$$\tau = \frac{2L}{Nv} \tag{2.23}$$

where N is the number vibration nodes (N=1,2,3,...,10) and v is the speed in the loop. The sound speed (v_s) is typically around 200 km/s and the Alfven speed (v_A) is around 400-1000 km/s [Roberts 2000] and [Nakariakov and Stepanov 2007]. Taking into account all wave modes (magnetoacoustic, Alfven, slow and fast MHD waves), the oscillation periods vary between 3 and 15 minutes when the loop length is 100 Mm. Shorter periods are also possible with higher vibration nodes. And if the loop length is 300 Mm, the periods are three times longer with a maximum of 45 minutes. Additionally, the so-called sausage modes cause oscillations, which are related to the oscillation loop radius. The equation for sausage mode periods can be written as

$$\tau = \frac{2\pi a}{j_0 v_A} \approx \frac{2.62a}{v_A} \tag{2.24}$$

where v_A is the Alfven speed within the loop, $j_{0,s}$ are the zeros from the Bessel function (2.4, 5.52,...), and a is the loop cross section radius (typically 1000 km, [Roberts 2000]). These sausage mode periods are around a few seconds. These periods may be able to explain some oscillation structures in the solar flares.

The MHD wave theory can explain a wide range of solar oscillation periods in the (coronal) loop structures. However, the main limitation is that periods above 45 minutes can not be explained with the MHD theory. The ideal MHD theory does not take into consideration gravitational effects. That is why we should also investigate other oscillation models (such as the shallow sunspot model in Chapter 3).

2.1.5 Propagating acoustic waves

The 3-minute sunspot umbral oscillations at radio wavelengths have been suggested to be cause by acoustic waves generated in the lower atmosphere. The waves are further propagating upward into the gyroresonance layers, where microwave radiation can be detected (the transition and coronal regions). Oscillations are expected to occur at certain frequencies above to the cutoff frequency (f_0) is defined as

$$f_0 = (g/4\pi)\sqrt{\frac{\gamma\mu}{RT}} \tag{2.25}$$

where $\gamma = 5/3$, μ is the mean molecular weight (=1.5), g is the gravity, R is the gas constant and T is the temperature. Thus the cutoff frequency only depends on the temperature. 5.6 mHz (3 minutes) corresponds to 3000 K umbral temperature. The lower frequencies can not propagate upward. Various observations (at 17 GHz, Nobeyama RadioHeliograph) support this interpretation [Shibasaki 2001].

Chapter 3

Sunspot models

3.1 Sunspot models

3.1.1 The standard (Parker) sunspot model

The traditional sunspot model [Parker 1979], known also as the Parker model or the cluster model, is presented in Figure 3.1. The continuous arrows illustrate the magnetic field lines (flux tubes), which are bundled together around 1000 km below the solar surface, caused by plasma downflows (dashes arrows) from the surface. Above this level (1000 km) magnetic field bundles (flux tubes) freely spread to several single flux tubes. Each flux tube is filled with cool plasma, and they have a strong magnetic field, a few thousands Gauss. The model does not take into accout the deep structure of the sunspot, for instance where and how the flux tube bundles are formed.

3.1.2 The shallow sunspot model

Various long quasi-periodic oscillations (40-200 minutes) have been detected in the sunspots, such as [Efremov et al. 2011], [Smirnova et al. 2011] and [Kallunki and Riehokainen 2012]. The physical interpretation of these oscillations may be completely different from explaining them with physical interpretaion of MHD oscillations. For the long oscillation periods, instead of traditional MHD model, we have to take into account the so-called shallow sunspot model by [Soloviev and Kirichek 2009],
[Soloviev and Kirichek 2008]. Some simulation models also agree with the shallow sunspot model [Rempel et al. 2009]. In Figure 3.2, the shallow sunspot model structure is shown. Two basic parameters influence the

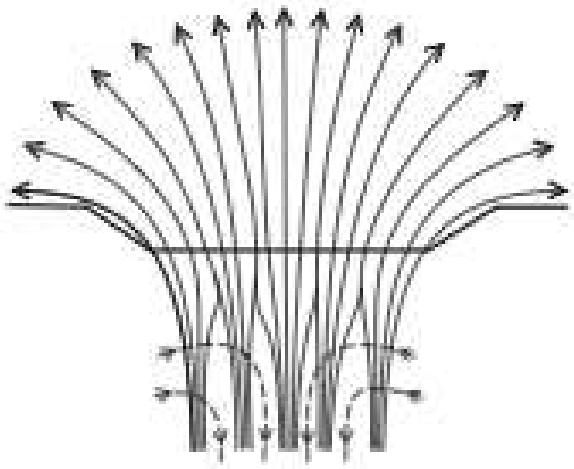

Figure 3.1: The Parker sunspot model [Kosovichev 2010].

shallow sunspot oscillations: the strength of the magnetic field in the quasi-cylindrical part of the sunspot flux tube and the mass of the plasma involved in the oscillations.

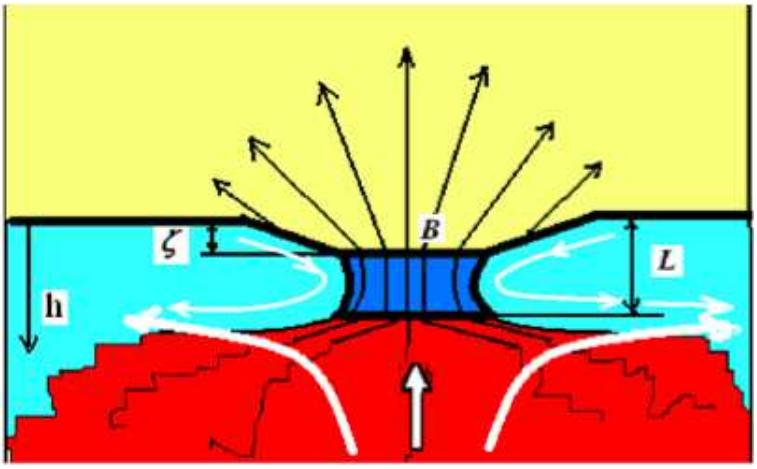

Figure 3.2: The shallow sunspot model suggested by A. Soloviev, which is also in accordance with the results of [Kosovichev 2006].

Between the depths ζ and L ($\sim$ 4 Mm) the magnetic field has a cylindrical geometry, while below that level the magnetic fields spread irregularly (the red area in Figure 3.2, where the temperature is higher). ζ is the Wilson depression and L is the sunspot depth. Starting from depths around 4000 km (the blue area in Figure 3.2), the gas temperature exceeds the ambient temperature. Thus, we can assume that the magnetic pressure is negligible. The white lines show plasma convection in the sunspot layers, which plays an important part for the long period oscillations.

At depths $h < L$ the plasma flows are directed towards the sunspot and at depths $h > L$ the flow is opposite. The speed of the flow is rather slow (around 1 km/s). However, these flows change the geometric structure of the sunspot magnetic field and further cause sunspot oscillations. These flows cause variations in the sunspot radius (a) and also changes in the depth of the Wilson depression. Two different structural physical processes define the sunspots: the vertical redistribution of gas masses (gravitational energy) and the energy of the magnetic fields. They can be assumed to be of the same order of magnitude, so that the relation can be written as

$$\frac{B^2}{8\pi}\pi a^2(L-\zeta) \cong \Delta M g(L-\zeta) \tag{3.1}$$

where $\Delta M g(L-\zeta)$ is the vertical redistribution of gas masses and ΔM is the moving gas mass. For the moving gas, we can assume $\Delta M \approx \pi a^2 \rho(0)\Lambda$, where Λ is the scale heigth in the photosphere at the level of the Wilson depression ($\Lambda \approx 200$ km). ρ_0 is the density of photospheric gas (5 x 10^{-7} g/cm^3). Therefore, we can obtain

$$B \cong \sqrt{8\pi G \rho(0)\Lambda} \tag{3.2}$$

where G is the gravitational constant. The frequency of oscillations of the sunspot as a whole can be calculated as

$$\omega \approx \frac{v_A}{L} = \frac{B}{L\sqrt{4\pi\rho_0}} \tag{3.3}$$

where v_A is the Alfven speed averaged over the spot depth, L is the sunspot depth (4 x10^8 cm), B is the magnetic field strength (2600 G) and $\rho_{0,1}$ is the mass density averaged over the depth of the sunspot ($\rho_{0,1} \approx 10\rho_0$). Equation 3.3 gives a period of around 100 minutes ($T = \frac{2\pi}{\omega}$). Thus, the periods are strongly related to the magnetic field strength and also the depth (L) has an effect on the periods. Also the second ($\omega/2$) and the third lower harmonics ($\omega/3$) are possible when the penumbra is involved in the oscillation process. A full detailed description of the shallow sunspot model (oscillation periods up to 11 hours) is given in [Soloviev and Kirichek 2013].

Based on the shallow sunspot model, two different mechanisms for the long quasi-periodic oscillations above the sunspots at radio wavelengths have been suggested; first, the mechanism for the modulation of radio emission at high levels is the magnetohydrostatic rebuilding of magnetic structures caused by slow time variation of the boundary field. In other words, any variations in the sunspot magnetic field cause a relatively rapid adjustment of the spatial structure in the active region that is connected with the magnetic flux of the sunspot. As we know, for instance, the coronal loop length can be as large as 100-300 Mm, which can further extend to the transition region and the corona (radio emission, Figure 1.2). This means that all physical parameters (temperature, density, pressure and the magnetic field) in the region where the radio emission is generated are changing, based on the variations of the field at the base level (the photosphere). Thus, the changes in the radio emission intensity are directly related to the changes in the sunspot field-time variations. Also, it has been shown that there is a phase difference in oscillation periods between the sunspot and the radio emission. The radio emission oscillations were delayed by about 15 minutes compared to the oscillations in the magnetic field strength of the sunspots [Smirnova et al. 2013].

A second mechanism for the modulation of radio emission was suggested by [Kshevetskii and Soloviev 2008]. They showed that the internal gravity waves propagate from the source at a small angle to the photosphere and the maximum of their density is reached at the height of about 3000 km, the region of 8 mm radio emission (in agreement with the Vernazza model of atmosphere). The maximum of the radio intensity, in this case, should be shifted from the centre of the sunspot by at least a few tens of thousands of kilometres sidewards.

Both of these mechanisms can explain, in principle, together or inde-

pendently the amplitude modulation of radio emission by slow long periodic oscillations of sunspots.

Chapter 4

Radio emission mechanisms

4.1 Introduction to the the radio emission mechanisms

The radio emission mechanisms can be divided into two different categories: coherent (the phase is stable) and incoherent (the phase is not stable) emissions. The incoherent emissions include bremsstrahlung (free-free) and gyroemission processes. The coherent emissions are plasma emission and electron cyclotron maser emission. Bremsstrahlung and gyroemission are the most interesting radiation processes because they can both be seen at radio frequencies, especially at centimeter and millimeter wavelengths. Bremsstrahlung is the prevailing incoherent emission mechanism in the areas where the magnetic field is negligible [Mercier and Chambe 2009], and also at mm-wavelengths when the magnetic field strength is below 100 G [Brajša et al. 2009]. In contrast, in the active regions (sunspots) both mechanisms are found; gyro-resonance emission above the sunspots at mm-wavelengths ([Shibasaki et al. 1994]; [Brosius and White 2006]) and free-free radiation from plasma in the active region loops [Shibasaki et al. 2011]. It has been shown [Nakariakov and Ofman 2001] that in the coronal loops the magnetic field strength varies between 4-30 G, which is much less than at the photospheric level.

4.2 Basics of Bremsstrahlung

Bremsstrahlung (also known as a braking or acceleration radiation or free-free radiation) radiation occurs when a charged particle accelerates by the force caused by another charged particle. The connection (source function,

S_ν) between emission (ϵ) and absorption (α) coefficients can be expressed by Kirchhoff's law in the case of Maxwellian electron distribution of temperature T

$$S_\nu = \frac{\epsilon}{\alpha} \tag{4.1}$$

For the radio frequencies, we can use the Rayleigh-Jeans approximation ($h\nu << kT$). The brightness (black body radiation at certain frequency) and effective (radiating electrons) temperatures (for radio frequencies) can be defined as

$$T_b = \frac{c^2}{2\nu^2 k} I_\nu \tag{4.2}$$

$$T_{eff} = \frac{c^2}{2\nu^2 k} S_\nu \tag{4.3}$$

where c is the velocity of light, ν is the frequency, k is the Boltzmann constant and I_ν is the specific intensity. The total radiation is the result of the emission and the absorption, thus the radiative transfer equation can be written in terms of the brightness temperature T_b [Dulk 1985]

$$\frac{dT_b}{d\tau_\nu} = -T_b + T_{eff} \tag{4.4}$$

where T_{eff} is the effective temperature of the radiating electrons and τ_ν is the optical depth. The solution of the equation 4.4 can be written as

$$T_b = \int_0^{\tau_\nu} T_{eff} exp(-\tau_\nu) d\tau_\nu + T_{bo} exp(-\tau_\nu) \tag{4.5}$$

where T_{bo} is a background brightness temperature. In the special case of an isolated source with constant T_{eff} the equation can be written in the simple form

$$T_b = T_{eff}[1 - e^{-\tau_\nu}] \tag{4.6}$$

For optically thin sources ($\tau << 1$) the brightness temperature can be written as

$$T_b = \tau_\nu T_{eff} \tag{4.7}$$

For optically thick sources ($\tau >> 1$) it can be assumed that $T_{eff} = T_b$. The relation between the optical depth and the absorption coefficient (α) can be written as

$$d\tau_v = \alpha ds \tag{4.8}$$

where ds is the distance. The free-free absorption coefficient α can be written as [Aschwanden 2006]

$$\alpha \approx 9.786 * 10^{-3} \frac{n_e \sum_i Z_i^2 n_i}{\nu^2 T^{3/2}} ln(\Lambda) \tag{4.9}$$

where ν is the radio frequency, n_i is the ion density, n_e is the electron density, Z is the atomic charge number and $ln(\Lambda)$ is the Coulomb integral. The Coulomb integral for coronal temperatures ($T > 3 * 10^5$ K) can be written as [Aschwanden 2006]

$$ln(\Lambda) = 24.5 + ln(T_e) - ln(\nu) \tag{4.10}$$

where T_e is the electron temperature. For lower temperatures ($T < 3 * 10^5$ K) the Coulomb integral can be written as [Pohjolainen 2000]

$$ln(\Lambda(z)) = 18.2 + 1.5 * ln(T_e) - ln(\nu) \tag{4.11}$$

4.3 Gyroemission

The mechanism of gyroemission is the spiral motion (acceleration) of moving particles in the magnetic field, caused by the Lorentz force. This movement causes radiation, which is known as gyroemission. The frequency at which gyroemission can be seen is called the gyrofrequency. The gyrofrequency can be written as

$$\nu_B = \frac{eB}{2\pi mc} \approx 2.8 * 10^6 B \tag{4.12}$$

where e is the charge of the particle (usually electron), B is the magnetic field strength, m is the mass of the particle and c is the speed of light [Zirin 1988]. The energy distribution in gyrosynchrotron emission can be written as [Dulk 1985]

$$n(E) = KE^{-\delta} \tag{4.13}$$

$$K = (\delta - 1)E_0^{\delta-1}N \tag{4.14}$$

where N is the number of electrons per cubic centimeter, δ is the electron power law index (typically δ=4) and E_0=10 keV. T_{eff} can be written as

$$T_{eff} \approx 2.2 * 10^9 10^{-0.31\delta}(sin\theta)^{-0.36-0.06\delta}(\frac{\nu}{\nu_B})^{0.50+0.58\delta} \tag{4.15}$$

where θ is the viewing (emission) angle. For optically thick ($\tau >> 1$) sources it can be assumed that $T_{eff} = T_B$. For optically thin ($\tau << 1$) sources the flux density (S) can be written as [Pohjolainen 1996]

$$S = \frac{2k\nu^2}{c^2} \int T_B d\Omega = \eta_{eff} L\Omega \tag{4.16}$$

where η_{eff} is the gyrosynchrotron emissivity and L is the dimension of the source along the line of sight. η_{eff} can be written as [Aschwanden 2006]

$$\eta_{eff} \approx 3.3 * 10^{-24} 10^{-0.52\delta} B n_e (sin\theta)^{-0.43-0.65\delta} (\frac{\nu}{\nu_B})^{1.22-0.9\delta} \tag{4.17}$$

where n_e is the electron density. Above mentioned approximations are valid with following conditions: $2 \leq \delta \leq 7$,$\theta \geq 20$ and $10 \leq v/v_b \leq 100$ [Dulk 1985].

4.4 Plasma emission

Plasma emission is the most prevailing emission source in solar flares up to 3 GHz [Benz 2005]. Radio emission is two-phased process. At first, energized electrons can propagate in plasma along with magnetic field lines. Higher energy electrons are faster and these cause various waves (electron beams). These unstable electron beams then cause Langmuir waves, which further are converted to electromagnetic radiation via non-linear wave-wave interactions. The plasma radiation occurs at above the plasma frequency (Hz), ν_p or its second harmonic $2\nu_p$. The plasma frequency ν_p can be written as

$$\nu_p \approx 8.97\sqrt{n_e} \tag{4.18}$$

where n_e is the electron density.

Chapter 5

Instrumentation

5.1 Metsähovi radiotelescopes

Metsähovi RT-14

The Metsähovi RT-14 telescope at the Metsähovi Radio Observatory (MRO), Aalto University (Helsinki Region, Finland, GPS: N 60 13.04 E 24 23.35) has a Cassegrain type antenna with a diameter of 13.7 meters. The working range of the telescope is 2-150 GHz (13.0 cm-2.0 mm). The antenna provides full disk solar mapping, partial solar mapping and, additionally, the ability to track any selected point on the solar disk. The beam size of the telescope is 2.4 arc min at 37 GHz. The receiver is a Dicke type radiometer, thus the radiometer's own noise will be filtered out. For the temperature stabilization of the receiver, a Peltier element is used. The noise temperature of the 37 GHz receiver is around 280 K, and the temporal resolution during the observations is 0.1 s or less. The obtained data is recorded as intensity. Only the 37 GHz band was used for the solar radio observations presented in this thesis. The radio emission at 37 GHz comes from the chromosphere and the lower corona (the transition region). The Quiet Sun temperature at 37 GHz is around 7800 K. The full documentation of Metsähovi RT-14 for solar observations can be found from [Kallunki et. al. 2012].

The northern location of the radiotelescope enables long, continuous solar observations in the summer months (May-August). It is even possible to perform solar observations as long as 14 hours. This is a unique characteristic of Metsähovi RT-14 and it opens up the possibility of studying long quasi-periodic solar oscillations and other kinds of long-term solar variability. In Figure 5.1 a typical solar radio map obtained with MRO RT-14 at

37 GHz is shown. The map consists of 30 sweeps over the solar disk. An example of the solar tracking observations is also shown.

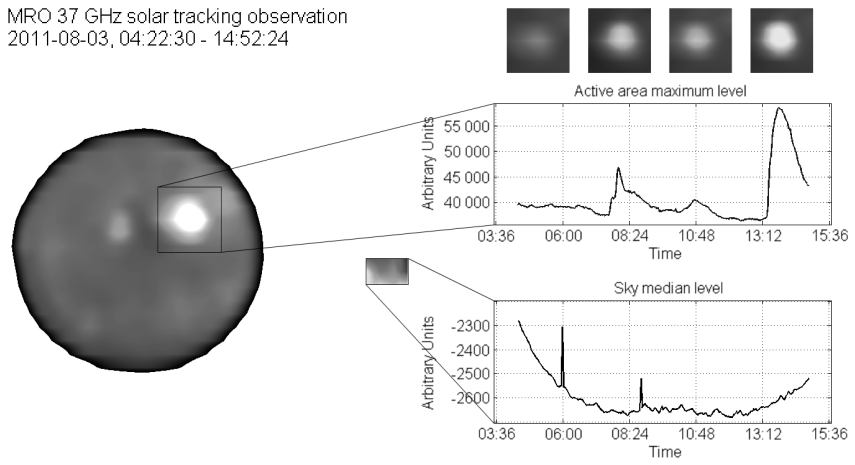

Figure 5.1: A solar radio map observed with Metsähovi RT-14, with an example of solar tracking observations.

When studying long period (∼5 minutes and longer) solar oscillations, solar tracking observations of the selected source (usually a radio brightening) are necessary. Continuous partial solar maps are observed over the active area (the radio brightening), and between every two maps a short scan of the sky is made. The cadence between two consecutive solar maps is about 1-2 minutes, depending on the size of the active region mapped. The sky scans enable us to study instrumental and sky effects and to remove their influence on the solar oscillations. Thus, the results can be calibrated reliably. We can also obtain full solar radio maps, but the cadence between two consecutive solar maps is then 7-8 minutes.

Metsähovi RT-1.8

Metsähovi Radio Observatory has also a small radiotelescope with a 1.8 m dish diameter (beam size 81.6 arc min). It observes the Sun's total radiation at 11.2 GHz continuously. The radiotelescope is used for observing solar radio bursts, and some studies on solar oscillations have also been

done. The high sampling rate (5 kHz) enables the study of flare fine structure, including short periodic oscillation phenomena. The radiotelescope has no protective radome, therefore it is vulnerable to prevailing weather conditions. The full documentation of Metsähovi RT-1.8 can be found in [Kallunki 2009].

[Khodachenko et al. 2011] studied solar oscillations during a solar radio burst (flare) using Metsähovi RT-1.8 data. They found various oscillation periods between 1.9 and 12.8 minutes (see an example in Figure 5.2). They assumed that some of these periods corresponded to the signatures of large-scale transverse oscillations of coronal loops.

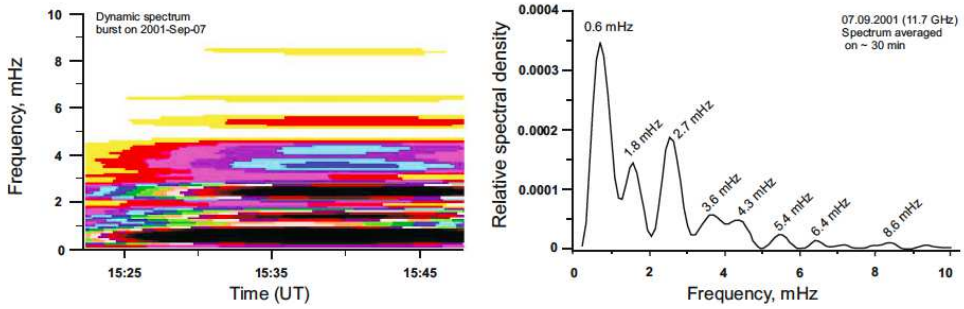

Figure 5.2: Oscillation analysis (FFT and Wavelet) of the observed solar radio burst (September 7, 2001), [Khodachenko et al. 2011].

Metsähovi - Callisto radio spectrometer

Metsähovi Radio Observatory joined the worldwide solar radio burst observing network (e-Callisto) in the fall of 2010. The network is coordinated by ETH Zurich and it consists of 22 different observing nodes (as of January 22, 2012) all over the world, covering solar radio spectral observations 24 hours a day throughout the year [Callisto 2012]. The network focuses on the decimeter and meter wavelength range. Callisto is a low cost radio spectrometer which uses, for instance, a normal TV tuner for sampling. The first solar radio bursts in Metsähovi were observed September 24th 2010 [Kallunki et. al. 2012].

The current frequency coverage in Metsähovi is 50-1450 MHz (the lower band is 50-846 MHz and the higher band 790-1447.250 MHz). After the

installation, over 100 solar radio bursts have been observed in MRO [Callisto-gallery 2012]. As an example, in Figure 5.3 the radio spectrum of one strong solar radio burst is shown. A slightly drifting emission can be observed over a wide frequency range (200-800 MHz).

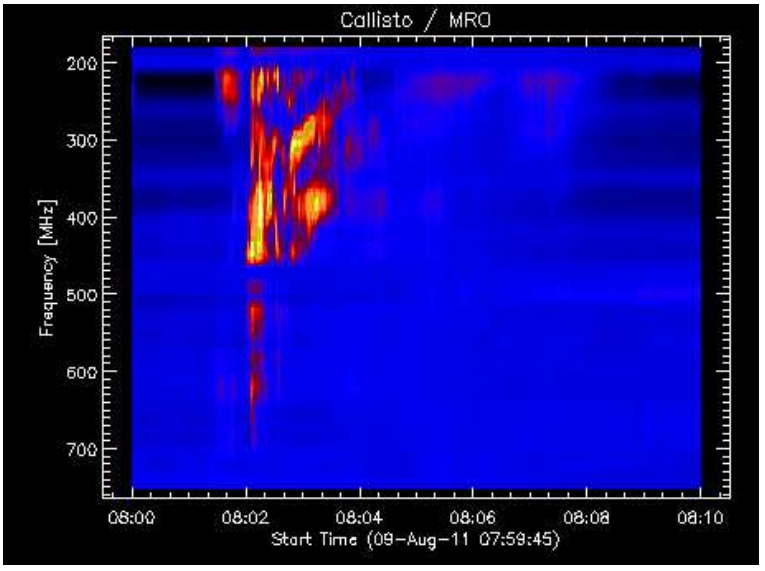

Figure 5.3: A strong solar radio burst observed with the Callisto measurement system at MRO at August 9, 2011.

Due to the low instrumental sensitivity studies of the quiet Sun are not possible.

5.2 Nobeyama Radioheliograph

Nobeyama Radioheliograph (NoRH) in Japan (Nagano region, GPS: N 35 56.34 E 138 28.26) is an instrument operating at the frequencies of 17 GHz and 34 GHz. In this thesis, only the 17 GHz (1.76 cm) band is used. The Radioheliograph consists of an array of 84 parabolic antennae and the diameter of one single antenna is 80 cm. The spatial resolution is 15 arcsec (at 17 GHz) over the whole solar disk. The NoRH is a radio interferometer and the full solar radio image is obtained by inverse Fourier transformation of visibilities measured by pairs of antennas. In Figure 5.4, an example

of a solar radio map from Nobeyama Radioheliograph is presented. The intensity is recorded in brightness temperature (Kelvin). The Quiet Sun temperature at 17 GHz is around 10000 K. Visibility data are taken and stored every 1 second (or 0.1 second) and images are synthesized over an interval which depends on the research purposes. Each day, observations are made in the UTC time interval 22:45-6:45 [Nobeyama 2012].

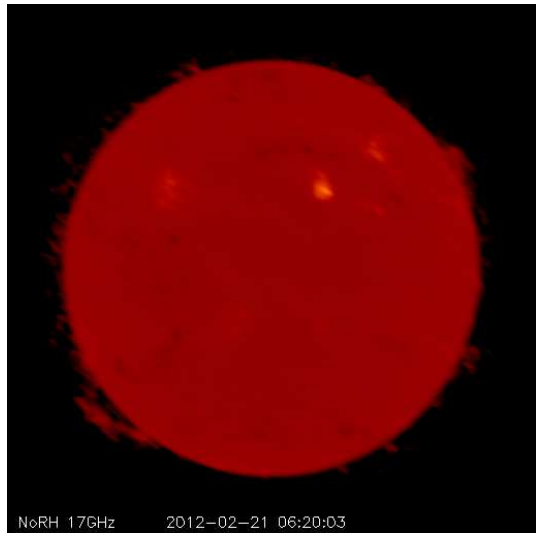

Figure 5.4: A solar radio map obtained with the Nobeyama Radioheliograph at 17 GHz [Nobeyama 2012].

Data from NoRH have also been used in several solar oscillation investigations. A relatively high resolution at radio wavelengths enables us to study oscillations in different solar fine structures.

5.3 SOHO/MDI

The SOHO (Solar & Heliosphere Observatory) / MDI (Michelson Doppler Imager) is an instrument to study photospheric structures (the longitudinal or the line-of-sight component of the magnetic field). As a satellite instrument, it is unaffected by atmospheric conditions. Further, it is an instrument which was primarily developed to study helioseismology and solar oscillations. The MDI is tuned to the Ni I (6768 Å) solar absortion

line with a bandbass of 94 mÅ. The MDI creates full-disk magnetograms (see an example in Figure 5.5) with varying cadences. The daily synoptic maps are recorded at intervals of 96 minutes, giving 15 synoptic maps each day. The SOHO/MDI maps have a resolution of 1024 pixels x 1024 pixels. The spatial resolution of the SOHO/MDI magnetogram is 4 arcsec over the whole solar disk. The magnetogram maps are saved in .FITS format. Level 1.8 magnetograms are short-term campaign observations, therefore they cover only a few hours time intervals [Scherrer et. al. 1995].

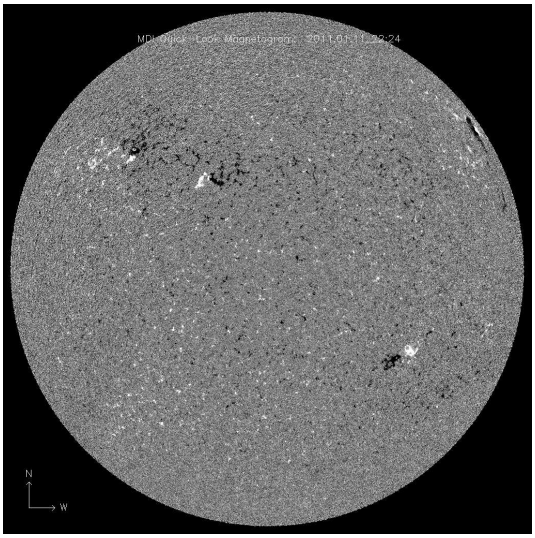

Figure 5.5: A MDI full-disk magnetogram, observed January 11, 2011 [SOHO/MDI].

5.4 Other radio instruments

The millimeter wavelength data (93 GHz) were obtained from the RT-7.5 radiotelescope (Cassegrain-type antenna with a diameter of 7.75 meters) belonging to the Bauman Moscow State Technical University (BMSTU, Moscow Region, Russia). The beam size of the telescope is 1.7 arcmin and the temporal resolution is 0.125 s [Smirnova et al. 2011]. The instrument enables us to do simultaneous observations together with RT-14 (MRO).

Solar radio events were analysed using three other instruments. The Bumishus solar radio polarimeter, operating at frequencies 8.4, 11.8, 19,6 and 35.0 GHz (90 GHz), was used for analyzing solar radio burst data in the millimeter and centimeter ranges. The data for the July 20, 2004 event is presented in Figure 5.6. The time resolution is of the order of 0.1 sec [Pohjolainen 1996].

The Phoenix-2 spectrogram was used for observing the Sun's full desimetric radio emission at 0.1-4 GHz (Figure 5.6). The radiotelescope has a 7 meter dish. The sampling time in each channel is 0.1 sec [Benz et al. 2011].

Additionally, Nancay Radioheliograph (NRH) radio images were used to analyze solar radio bursts. NRH is an interferometer consisting of of 44 antennae, whose dishes vary in diameter from 2 to 10 meters. The resolution of NRH maps is around 2 arc min. The cadence between two consecutive solar radio maps is 0.15 sec [Klein et al. 2008].

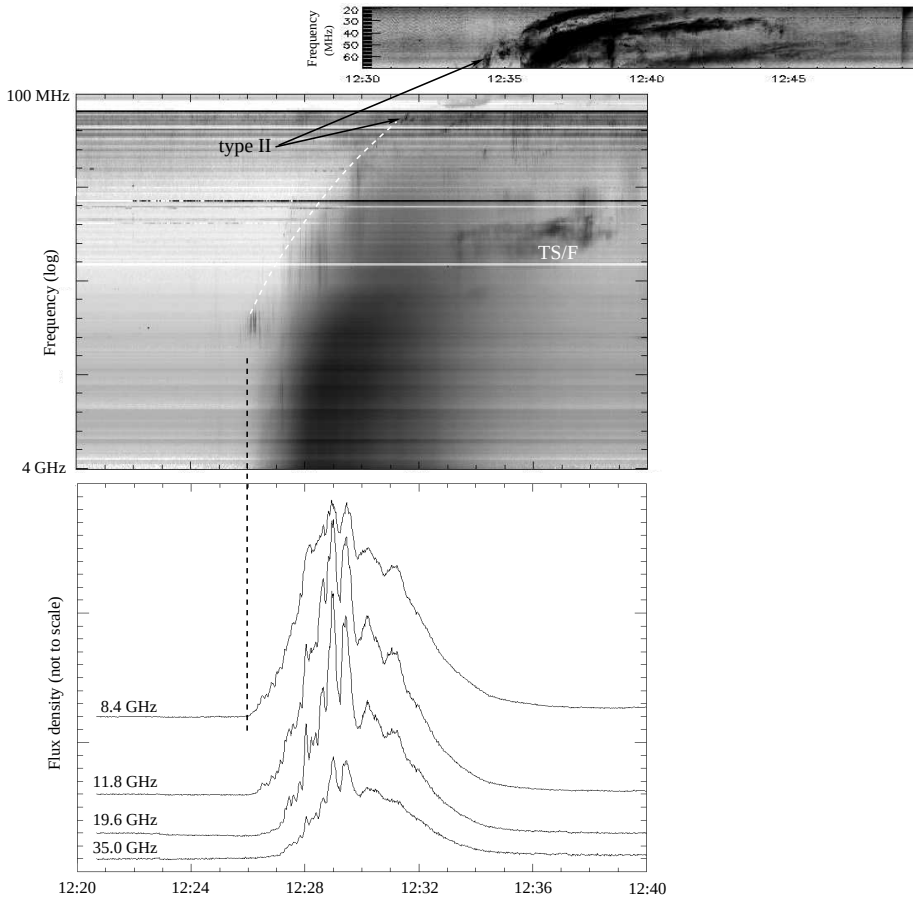

Figure 5.6: Upper plot: Green Bank Solar Radio Burst Spectrometer, GB-SRBS (70 – 20 MHz). Middle plot: Phoenix-2 (0.1-4 GHz). Lower plot: Bumishus (8.4, 11.8, 19,6 and 35.0 GHz) [Kallunki and Pohjolainen 2012], Article V.

Chapter 6

Data analysis

6.1 Periodicity analysis

To find out periodicities in the observed solar data, the Fast Fourier Transform (FFT) method and the Wavelet analysis, along with the Global Wavelet Spectrum (GWS), were chosen. Further, the Morlet Wavelet (6th order) was chosen to analyze the data [Torrence and Compo 1998]. These two different types of analysis can reveal both stationary and transient signals (the global method, FFT) and long-lasting signals (the local method, Wavelet). In the FFT analysis we used different window functions for each data set from different instruments in order to minimize the FFT response to noise (the level of noise and the sampling rates were different for each instrument). Further, the significance levels of each data set were assessed.

6.1.1 Fast Fourier Transform (FFT)

The Fourier Transform of the function $f(x)$ can be defined as

$$f(\omega) = \int_{-\infty}^{+\infty} f(x) e^{-i\omega x} dx \tag{6.1}$$

where $e^{-i\omega x} = \cos(\omega x) + \sin(\omega x)$ (Euler's formula). In this thesis, Matlab's™ fft-function is used, which further uses the Fast Fourier Transform algorithm. The FFT is defined as

$$f(\omega) = \frac{1}{N} \int_{j=1}^{N} f(x) \omega_N^{-(j-1)(k-1)} dx \tag{6.2}$$

where N is number of samples, $k = 0, ..., N-1$ and $\omega_N = e^{(-2\pi i)/N}$. Additionally, various windowing (filtering) methods are used for the analyzed signals, depending on the situation and the instrument. In general, in this thesis we are focusing on the periods, which are around four times smaller than the Nyqvist frequency in each data set. As is well known, the traditional FFT can not reveal quasi-periodicity unlike windowed FFT.

6.1.2 Wavelet transform

The Wavelet analysis is an efficient method for investigating periodicity phenomena in a signal, and, furthermore it also reveals quasi-periodicities. Furthermore, it enables us to study signal behaviour both in the time and in the frequency domain. The basic idea of the Wavelet Transform is that the analysed signal will be scanned with desired mother function (Ψ) while changing the time delay (τ) and the scale parameter (s). The continuous Wavelet transform is defined as

$$\Psi(\tau, s) = \frac{1}{\sqrt{\mid s \mid}} \int_{-\infty}^{+\infty} x(t) \Psi^*(\frac{t-\tau}{s}) dt \tag{6.3}$$

(*) indicates that the complex conjugate is used in the case of a complex Wavelet. In this thesis, the Morlet Wavelet was used as a mother function. The Morlet mother function is defined as

$$\Psi(t) = \pi^{1/4} e^{i\omega_0 t} e^{-t^2/2} \tag{6.4}$$

where ω_0 is the central frequency of the Morlet Wavelet. In this thesis, the value of s was taken to be 6 (6th order Morlet Wavelet). In Figure 6.1 an example of the results of a Wavelet analysis is presented.

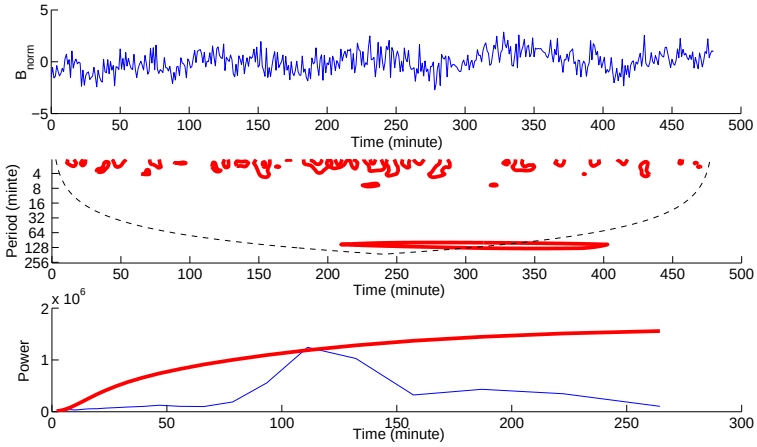

Figure 6.1: An example of periodicity analysis (NoRH on July 3, 2008). Upper panel: the normalized data set. Middle panel: The Wavelet analysis. The thick red contours indicate the 99 % confidence levels. Lower panel: The Global Wavelet spectrum. The thick red line indicates the 99 % confidence level [Kallunki and Riehokainen 2012], Article I.

6.2 Significance tests

It is important to study the significance of the analyzed signals, especially of weaker signals, such as quiet Sun area (QSA) signals, which often can resemble random noise. This is one possible way to separate the real oscillation phenomena from, for instance, the instrumental effects.

Significance levels of Fourier and Wavelet spectra

Two different approaches were chosen to study the significance of spectra. A simple method was to define the variance (σ) of the Fourier spectrum and further choose some significance level based on the variance. Typically, the level was chosen to be 3σ, thus periods above this level were considered to be significant.

The more advanced method is based on the model by [Torrence and Compo 1998]. White and red noise spectra, based on the original signal, are constructed using an appropriate lag-1 autocorrelation. The final, mean spectra are generated as the sum of 100 000 such spectra.

The original spectrum can then be compared with this generated mean spectrum with various confidence levels. Depending on the analyzed data set, either 95 % or 99 % confidence level, or both, was used.

Fisher randomization

To verify that the observed signal is not just random noise, we used the bootstrapping method (also known as the Fisher randomization test). The basic idea of this test is that the data points of the observed signal will be mixed randomly. Thus, new signals consist of the points of the original signal, which are randomly placed at time positions different from the original signal. 1000 randomization rounds were made for the signal. Further, the periodicities of these 1000 new generated signals were studied and compared to the periodicities of the original signal. Finally, we estimated the probability of how often periodicities occur in the randomly generated signals. Typically, significance levels below 0.05 were assumed to show that periods are real. This is a quite similar method as was presented for the spectral significance analysis.

6.3 Data post-handling

The data sets for analysis were typically constructed by selecting some area or object of interest (a sunspot, an active region or a QSA) from the radio images obtained from Nobeyama, BMSTU and Metsähovi, or from the magnetogram (SOHO / MDI). Within the selected area, usually the maximum, the minimum, or the average value of the studied variable was measured, along with the size of the selected area. Thus, based on the consecutive solar images or maps, several time series were obtained for the analysis.

All the data sets were scaled with their variance, which simplifies the comparison between data sets. Before the periodicity analysis, the long data sets (>24 h) were corrected with the differential rotation parameters of the Sun.

The periodicity analysis was performed using the methods presented earlier. In addition to the common periods, other key parameters between the data sets were also investigated, like the variation range (min-max difference) and the variance. Furthermore, in some cases a cross-correlation analysis between the signals was performed.

Each instrument also has unique technical features, which might influence the oscillation period analysis. Also the weather is a common problem with ground-based instruments. [Raju et al. 2001] has shown that SOHO/MDI has a shutter noise period of 96 minutes, which should be taken into account in the final conclusions and analysis. Moreover, the analysis methods might give some artifacts. Thus solar oscillations form the complex physical ensemble, which needs various theoretical analyses and interpretations. A main challenge is to find a way to separate periods from real oscillation structures and various artifacts.

Chapter 7

Conclusions and summary of publications

The main goal of this thesis is to investigate quasi-periodic solar oscillations (with periods larger than 3 minutes) in various atmospheric structures (Chapter 1), focusing mainly on sunspots (Articles II and III). Investigations were realized using several instruments at radio wavelengths (centimeter and millimeter) as well as magnetograms (6768 Å). Studies revealed interesting oscillation periods, especially longer ones: 35–70, 90 minutes (QSA) and 10-60, 80-130, 220-240, 340 and 470 minutes (sunspots). In this thesis two different theoretical approaches (magnetohydrodynamics, Chapter 2, and the shallow sunspot structure model, Chapter 3) have been used to derive physical interpretations of oscillations in sunspots (Article I) and also in other atmospheric structures (Article IV). Using these frameworks, it is possible to explain a wide range of oscillation periods. MHD theory (flux tubes) can explain the shorter detected periods (<45 minutes), while the shallow sunspot model can explain the longer periods. The solar oscillations detected in this thesis were confirmed using various instruments and wavelengths (Chapter 5), concentrating on radio wavelengths. Furthermore, all the detected oscillation periods have been confirmed by other research groups. The radio emission mechanisms were presented in Chapter 4. The data analysis methods were presented in Chapter 6.

Another related research area of this thesis was to develop new solar instrumentation. Thus, a relatively high emphasis is given to solar instrumentation (Chapter 5, Article VI). Finally, long-term solar cyclicity was studied at the radio frequency of 37 GHz (Article V).

In the sections below the scientific results from the articles included in

this thesis will be introduced.

7.1 Solar oscillations at QSA - Article I

Solar oscillations in the QSAs were studied using data from the Nobeyama Radioheliograph at 17 GHz. QSA oscillation periods were analysed with statistical methods. Areas of varying sizes were chosen from the quiet solar disk (B $<$ 200 G), and altogether 140 time series were constructed. The maximum, the minimum, and the average values of brightness temperatures of the selected areas were used as the variables for analysis. Periodicity analysis was performed for each resulting time series. The frequency of occurrence of each detected oscillation period in the 140 time series was calculated. The statistical distribution of various oscillation periods in QSAs is presented in Figure 7.1.

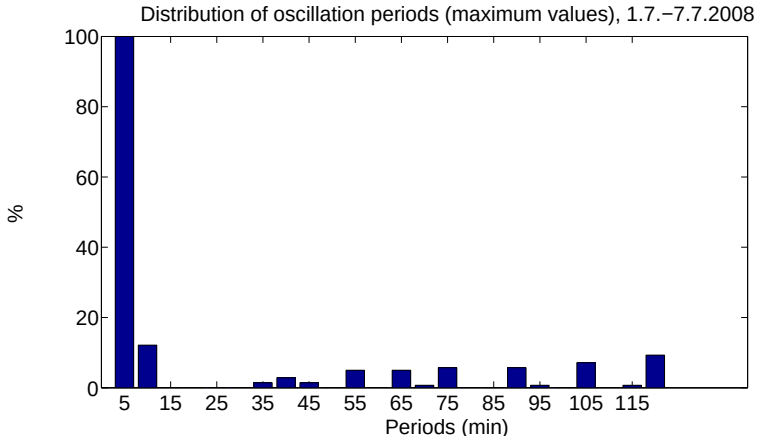

Figure 7.1: Distribution of the observed solar oscillation (NoRH) periods, based on GWS analysis (confidence level 95 %). Oscillations are grouped into 5 minute intervals. The distribution is the result of 140 time series. 100 % indicates that an oscillation period was found in every time series [Kallunki and Riehokainen 2012], Article I.

Based on these statistics, and also taking into account other factors, it is possible to conclude that QSAs at 17 GHz include the following oscillation periods: 3–15, 35–70, and >90 minutes. The shortest periods, however, are

much more common.

The periods shorter than 45 minutes can be explained by flux tube structures, which are present at the boundaries of supergranulae structures, using various magnetohydrodynamic wave modes as was presented in Chapter 2.

Possible physical explanations for longer oscillation periods, which are beyond the traditional MHD theory, have been proposed by
[Kurths et al. 1988]. 90-minute oscillations have been suggested to come from the rotation of the supergranulation pattern.

This study is one of the few that focus on solar oscillations in the QSAs, especially at radio wavelengths. It is obvious that a reliable detection of QSA oscillations is a challenge. However, with the various data analysis methods (significance tests, etc.), this was possible to achieve.

More accurate instruments, such as the Hinode satellite and the Swedish Solar Telescope (SST), have revealed some new phenomena which are also present in the QSAs. Quiet Sun Jets (QSJ) are one example of these new solar atmospheric features [Martinez Pillet et al. 2011]. Such structures may have an effect on solar oscillations.

7.2 Sunspot oscillations - Articles II and III

Sunspot oscillations in active regions (AR) were investigated based on their radio emission (chromosphere, transition region and low corona) and also on magnetograms, from SOHO/MDI (photosphere). Various radio instruments and frequencies were used; 17 GHz (NoRH), 37 GHz (MRO) and 93 GHz (BMSTU).

In the summer of 2010, simultaneous radio observation campaigns were realized between the MRO and the BMSTU radiotelescopes to analyze sunspots oscillations. The observations and analysis revealed several common oscillation periods; 10-60 and 80-130 minutes (examples in Figure 7.2, MRO and Figure 7.3, BMSTU). These quasi-periodic oscillations were also confirmed by using data from NoRH [Smirnova et al. 2011]. Figure 7.2 shows oscillations at two different intervals: 16-60 and 80-130 minutes. These detected sunspot oscillations at radio wavelengths are quite consistent with previous studies [Dzhimbeeva 2011].

Sunspots at the photospheric level also revealed various oscillation periods: 3-5, 10-23, 220-240, 340 and 470 minutes

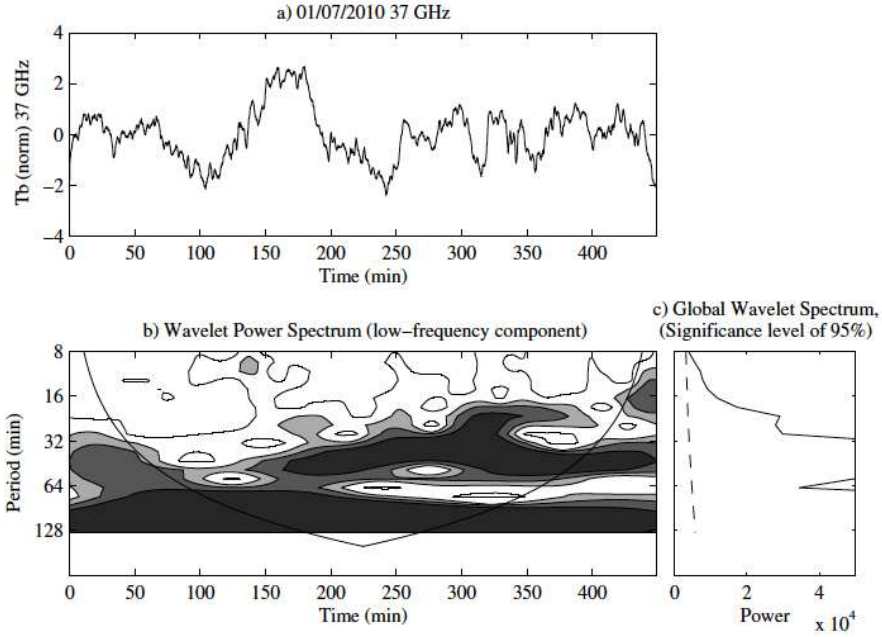

Figure 7.2: Periodicity analysis of AR 11084 (July 1, 2010) at 37 GHz using MRO data. Upper panel: The data track. Lower panels: the Wavelet spectrum and the GWS [Smirnova et al. 2011], Article II.

[Kallunki and Riehokainen 2012]. Similar periods have been found previously [Efremov et al. 2011]. The chosen sunspots had magnetic field strength values between 800 and 2200 G. An example of the periodicity analysis is shown in Figure 7.4.

Possible physical interpretations of sunspot oscillations were presented in Chapters 2 and 3. Short periods (< 45 minutes) are primarily related to various loop structures and MHD modes. The longer periods (> 45 minutes), and a part of the shorter periods, are however related to oscillations of the whole sunspots. Similar periods (10-23 minutes) were also detected in the sunspot area variations and also in the magnetic field strength (amplitude) changes. This supports the idea that some of these oscillations are related to global changes in the sunspot structure, as proposed by the shallow sunspot model.

Unfortunately, the sampling frequencies and the length of the data series

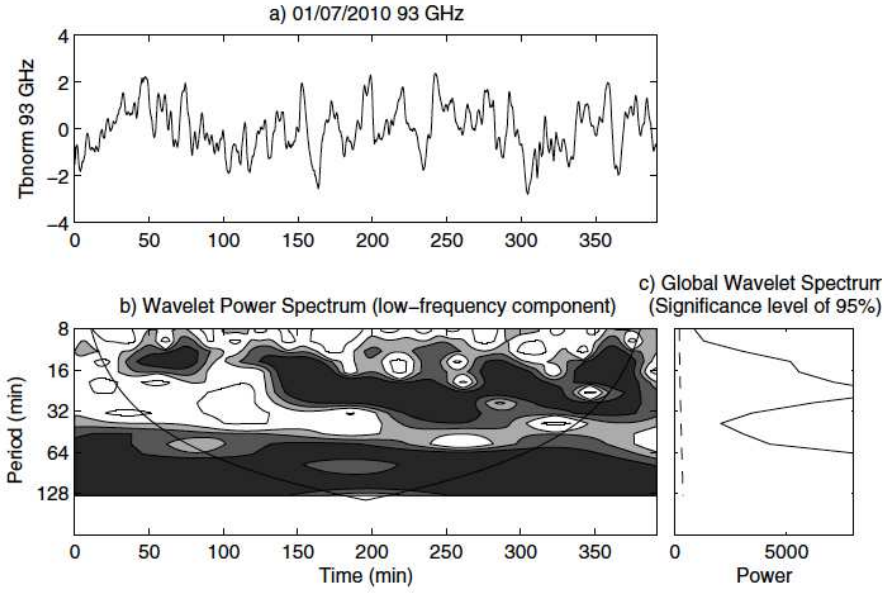

Figure 7.3: Periodicity analysis of AR 11084 (July 1, 2010) at 93 GHz using BMSTU data. Upper panel: the data track, Lower panels: Wavelet spectrum and GWS [Smirnova et al. 2011], Article II.

between SOHO/MDI and the radio instruments were different, and thus studying common periods was not entirely possible.

7.3 Quasi-Periodic Pulsations (QPP) - Article IV

A strong solar eruption event occurred on July 20, 2004, and at the same time a moving EUV loop was observed above the active region (NOAA AR 10652). The quasi-periodic pulsations (QPP) of this flaring event were investigated in the microwave, millimeter and desimeter ranges. Two different period intervals were detected: 8-12 and 15-17 seconds. The physical interpretation is that these periods are related to MHD oscillations (sausage modes) in the nearby EUV loops. Thus accelerating electrons cause radio emission. The theory of sausage modes was discussed in Chapter 2, and two possible flare-pulsating scenarios were shown in Chapter 1. Comparable periods with similar physical explanations have been reported

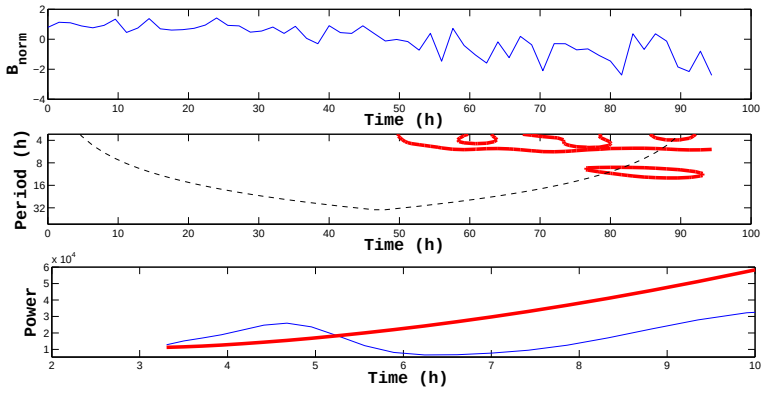

Figure 7.4: An example of our sunspot data analysis (00:00 (February 26, 2002) - 22:30 (March 3, 2002), NOAA: 09845). Upper panel: the normalized data set. Middle panel: the Wavelet analysis. Lower panel: the Global wavelet spectrum. The thick red contours indicate the 95 % confidence level [Kallunki and Riehokainen 2012], Article III.

[Nakariakov et al. 2003], [Asai et al. 2001] and [Pascoe et al. 2007].

7.4 Long-term solar activity - Article V

Solar radio observations have a relatively short history. The first instrumentation was available after World War II. However, full solar radio images have been actively obtained only for the past few decades. Metsähovi Radio Observatory has an extensively long history of these observations, and solar radio maps have been recorded since 1978. The variation of solar radio brightenings has been studied over three decades (two full solar activity cycles). We found that solar brightenings correlate quite strongly with the occurence of sunspots. However, some exceptions were noticed, mainly in the polar regions. This may result from polar faculae having their own cycle. Additionally, a rather good approximation for the differential rotation parameters of the Sun was derived, although the used resolution (2.4 arcmin at 37 GHz) was rather low. The instrumentation and the technical details were presented in Chapter 5, section 6.1.

7.5 New solar instrumentation - Article VI

The concepts of Callisto and the e-Callisto-network were demonstrated in Chapter 5. This article introduces the MRO Callisto measurement system's detailed implementation, including technical configurations and various test measurements, which were carried out together with the ETHZ. For instance, the local radio frequency interference (RFI) spectrum was measured. The technical portion of the work was completed in August-September 2010. The article also presents the first observed solar radio bursts on September 18, 2010 (a type III solar burst) and on September 24, 2010 (a type I solar burst). These bursts are created with the plasma emission mechanism, descripred in Chapter 4, section 5.4. The latter radio burst was a strong event, which was also picked up by various other Callisto instruments.

7.6 Future work

Our investigations have revealed a considerable amount of interesting quasi-periodic oscillations, especially those with longer periods (> 60 minutes). In the near future, we would like to continue to work with these long quasi-periodic oscillations both in sunspots and QSAs using our own instrumentation (Metsähovi RT-14). As was mentioned, solar observations (tracking an active area) longer than 12 hours can be achieved. Some preliminary results have already been obtained, but further investigations will be needed, including more observations and theoretical interpretations. The physical interpretation of these longer quasi-periodic oscillations is still partly unsolved, and thus there is a need for further investigations.

In addition, we would like to investigate oscillation phenomena in more detail, using the Solar Dynamics Observatory (SDO) satellite and the Helioseismic and Magnetic Imager (HMI) data. HMI's high spatital and temporal resolution enable studies of small structures such as pores and sunspot fine structures. This might, for instance, give a better physical explanation of the QSA oscillations, and it could even give new insights into the origin of solar oscillations.

Additionally, we will continue to work with QPPs by studying solar flaring events in order to confirm our physical interpretations. This project also includes instrumental development, such as of the Callisto measurement system. Some promising pulsating events have already been observed,

needing further analysis.

Other solar cyclicity analyses are also possible. The extensive Metsähovi data set from 1978 onward, at 37 GHz, makes this possible.

Bibliography

Abramov-Maximov, V. E., Gelfreikh, G. B., Kobanov, N. I., Shibasaki, K., and Chupin, S. A. 2011, Sol. Phys., 270, 175.

Andic A., Goode, P. R., Chae, J., et al. 2010, ApJ, 717, L79.

Antia, H. M. 2009, IAU Symposium, 257, 83.

Anzer, U., and Galloway, D. J. 1983, MNRAS, 203, 637.

Asai, A., Shimojo, M., Isobe, H., et al. 2001, ApJ, 562, L103.

Asai, A., Ishii, T. T., Isobe, H., et al. 2012, ApJ, 745, L18.

Aschwanden, M. J. 2006, Physics of the Solar Corona: An Introduction With Problems And Solutions, Springer Science Business.

Benz. A. 005, Sixth International Workshop on Planetary and Solar Radio Emissions Graz, April 20 - 22, 2005, (eds. H.O. Rucker, W.S. Kurth, G. Mann).

Benz, A. O., Battaglia, M., and Vilmer, N. 2011, Sol. Phys., 273, 363.

Brajša, R., Romštajn, I., Wöhl, H., et al. 2009, A&A, 493, 613.

Brosius, J. W., and White, S. M. 2006, ApJ, 641: L69–L72.

Callisto documentation - http://www.e-callisto.org/, 21.2.2012.

Callisto gallery in Metsähovi - http://www.metsahovi.fi/callisto-gallery, 21.2.2012.

Chorley, N., Hnat, B., Nakariakov, V. M., Inglis, A. R., and Bakunina, I. A. 2010, A&A, 513, A27.

Centre National d'Etudes Spatiales (CNES), http://www.cnes.fr, 6.5.2012.

Dulk, G. A. 1985, ARA&A, 23, 169.

Dzhimbeeva, L. N. 2011, Solar System Research, 45, 84.

Efremov, V. I., Parfinenko, L. D., and Soloviev, A. A. 2010, Sol. Phys., 267, 279.

Evans, D. J., and Roberts, B. 1990, ApJ, 348, 346.

Kallunki, J.: Possibilities of the Metsähovi radiotelescopes for solar observations, Helsinki University Of Technology, Faculty of Information and Natural Sciences, Licenciate Thesis, 2009.

Kallunki, J., and Riehokainen, A. 2012, Astronomische Nachrichten, 333, 20.

Kallunki J., Monstein C. and Uunila, M. 2013, The IEEE Aerospace and Electronic Systems Magazine, p.5-9, August 2013.

Kallunki, J., Lavonen, N., Järvelä, E. and Uunila, M. 2012, Baltic Astronomy, 21, 255.

Kallunki, J., and Pohjolainen, S. 2012, Sol. Phys., 101.

Kallunki, J., and Riehokainen, A. 2012, Sol. Phys., 116.

Kariyappa, R., and Damé, L. 2010, Mem. Soc. Astron. Italiana, 81, 786.

Karlicky, M., Barta, M. 2004, Nonlinear Processes in Geophysics (2004), 11, 471-483.

Khodachenko, M. L., Kislyakova, K. G., Zaqarashvili, T. V., et al. 2011, A&A, 525, A105.

Klein, K.-L., Krucker, S., Lointier, G., and Kerdraon, A. 2008, A&A, 486, 589.

Kontogiannis, I., Tsiropoula, G., and Tziotziou, K. 2010, 9th International Conference of the Hellenic Astronomical Society, 424, 31.

Kosovichev, A. G. 2006, Advances in Space Research, 38, 876.

Kosovichev, A. G. 2010, arXiv:1010.4927.

Kshevetskii, S. P., and Soloviev, A. A. 2008, Astronomy Reports, 52, 772.

Kurths, J., Aurass, H., Urpo, S., and Pohjolainen, S. 1988, A&A, 191, 359.

Leighton, R. B., Noyes, G. W. and Simon, G. W. 1962, ApJ, 135, 474.

Lou, Y.-Q. 1995, MNRAS, 274, L1.

Martinez Pillet, V., Del Toro Iniesta, J. C., and Quintero Noda, C. 2011, A&A, 530, A111.

Martinez Gonzalez, M. J., Asensio Ramos, A., Manso Sainz, R., Khomenko, E., Martinez Pillet, V., Solanki, S. K., López Ariste, A., Schmidt, W., Barthol, P., and Gandorfer, A. 2011, ApJ, 730, L37.

McKenzie, D. E. 2002, Multi-Wavelength Observations of Coronal Structure and Dynamics, 155.

Mercier, C., and Chambe, G., 2009 , 700, L137.

Nakariakov, V.M., and Ofman, L. 2001, A&A, 372, L53.

Nakariakov, V. M., Melnikov, V. F., and Reznikova, V. E. 2003, A&A, 412, L7.

Nakariakov, V.M., Foullon, C., Verwichte, E., and Young, N. P. 2006, A&A, 452, 343.

Nakariakov, V. M., and Stepanov, A. V. 2007, Lecture Notes in Physics, Berlin Springer Verlag, 725, 221.

Nobeyama radioheliograph - http://solar.nro.nao.ac.jp/norh/, 21.2.2012.

Pascoe, D. J., Nakariakov, V. M., and Arber, T. D. 2007, A&A, 461, 1149.

Parker, E. N. 1979, ApJ, 230, 905.

Pohjolainen, S., 1996, Doctoral thesis, Helsinki University of Technology, 1996.

Pohjolainen, S. 2000, A&A, 361, 349.

Raju, K. P., Singh, J., Srikanth, R., Chou, D.-Y., and TON team: 2001, Sol. Phys., 199, 1.

Rempel, M., Schüssler, M., Cameron, R. H., & Knölker, M. 2009, Science, 325, 171.

Roberts, B. 2000, Sol. Phys., 193, 139.

Scherrer, P. H., Bogart, R. S., Bush, R. I., Hoeksema, J. T., Kosovichev, A. G., Schou, J., Rosenberg, W., Springer, L., Tarbell, T. D., Title, A., Wolfson, C. J., Zayer, I. and MDI Engineering Team: 1995, Sol. Phys., 162, 129.

Shibasaki, K., Enome, S., Nakajima, H., et al. 1994, PASJ, 46, L17.

Shibasaki, K. 2001, ApJ, 550, 1113.

Shibasaki, K., Alissandrakis, C. E., and Pohjolainen, S. 2011, Sol. Phys., 273, 309.

Shibata, K., & Magara, T. 2011, Living Reviews in Solar Physics, 8, 6.

Smirnova, V., Riehokainen, A., Ryzhov, V., Zhiltsov, A., and Kallunki, J. 2011, A&A, 534, A137.

Smirnova, V., Riehokainen, A., Solov'ev, A., et al. 2013, A&A, 552, A23.

SOHO/MDI Data Services Information - http://soi.stanford.edu/data/, 6.5.2012.

Soloviev, A. A., and Kirichek, E. A. 2008, Astrophysical Bulletin, 63, 169.

Soloviev, A. A., and Kirichek, E. A. 2009, Astronomy Reports, 53, 675.

Soloviev, A. A., and Kirichek, E. A. 2013, Monthly Notices of Royal Astronomical Society (submitted)

Stix, M. 2004, The Sun : an introduction, 2nd ed., by Michael Stix. Astronomy and astrophysics library, Berlin: Springer, 2004. ISBN: 3540207414.

Torrence, C., and Compo, G. P. 1998, Bulletin of the American Meteorological Society, Vol. 79, No. 1, January 1998.

University Corporation for Atmospheric Research (UCAR), http://www2.ucar.edu, 6.5.2012.

Whang, Y. C. 997, ApJ, 485, 389.

Zirin, H. 1988, Astrophysics of the Sun, Cambridge University.